# Adaptive Range Identification for Exponential Visual Servo Tracking*

W. E. Dixon,[1] Y. Fang,[2] D. M. Dawson,[2] and J. Chen[2]

[1]Engineering Science and Technology Division, Robotics and Energetic Machines Group, Oak Ridge National Laboratory, P.O. Box 2008, Oak Ridge, TN 37831-6305

[2]Department of Electrical & Computer Engineering, Clemson University, Clemson, SC 29634-0915

E-mail: dixonwe@ornl.gov, Telephone: (865) 574-9025

Keywords: Homography, Range Identification, Visual Servo Control



To appear at the IEEE International Symposium on Intelligent Control, Oct. 5 - 8, 2003, Houston, TX

* This research was supported in part by the U.S. Department of Energy (DOE) Office of Biological and Environmental Research (OBER) Environmental Management Sciences Program (EMSP) project ID No. 82797 at Oak Ridge National Laboratory (ORNL), managed by UT-Battelle, LLC, for the DOE under contract DE-AC05-00OR22725, and in part by a University of Florida subcontract to ORNL by the Florida Department of Citrus, and by U.S. NSF Grant DMI-9457967, ONR Grant N00014-99-1-0589, a DOC Grant, and an ARO Automotive Center Grant.

# Adaptive Range Identification for Exponential Visual Servo Tracking*

W. E. Dixon†, Y. Fang‡, D. M. Dawson‡, and J. Chen‡

†Eng. Science and Tech. Div. - Robotics, Oak Ridge Nat. Lab., P.O. Box 2008, Oak Ridge, TN 37831-6305

‡Department of Electrical & Computer Engineering, Clemson University, Clemson, SC 29634-0915

E-mail: dixonwe@ornl.gov; ddawson, yfang, jianc@ces.clemson.edu

**Abstract:** A projective homography is developed by relating feature points extracted from images taken at the reference and current camera position/orientation. By decomposing the homography into translation and rotation components, geometric relationships are determined that facilitate the construction of an adaptive strategy to identify unknown depth information. The development of the parameter identification strategy provides a mechanism to develop a position-based and a hybrid position/image-based visual servo controller for a trajectory tracking control problem. By using information obtained from the parameter identification strategy, both visual servoing controllers are proven to yield exponential tracking.

## 1 Introduction

A significant issue that has impacted the development and application of visual servo control algorithms is the fact that the image-space is a 2-dimensional (2D) projection of the 3D task-space. To compensate for the lack of depth information from the 2D image data, researchers have explored the use of additional sensors (e.g., laser and sound ranging technologies) and the use of additional cameras in a stereo configuration that triangulate on corresponding images. However, the practical drawbacks of incorporating additional sensors include: increased cost, increased complexity, decreased reliability, and increased processing burden to condition and fuse sensor data. Motivated by these practical insights, recent research has focused on monocular visual servo strategies that do not require additional depth sensors. To achieve this objective, partitioned approaches that exploit a combination of reconstructed 3D task-space information and 2D image-space information have been proposed. For example, in the series of papers by Malis and Chaumette (e.g., [1, 2, 12, 13, 14]) various kinematic control strategies (coined 2.5D visual servo control) exploit the fact that the interaction between translation and rotation components can be decoupled through a homography. Information combined from the task-space (obtained through a projective Euclidean reconstruction from the image data) and the 2D image-space is utilized to regulate the translation and rotation error systems. In [6], Deguchi utilizes a homography relationship and an epipolar condition to decouple the rotation and translation components and then illustrates how two types of visual controllers can be developed from the decoupled information. Corke and Hutchinson [5] also developed a hybrid image-based visual servoing scheme that decouples rotation and translation components from the remaining degrees of freedom. One drawback of the aforementioned controllers are that each result claims (without a supporting proof) that a constant, best-guess estimate of the depth information can be utilized in lieu of the exact value. Motivated by the desire to actively compensate for unmeasurable depth information, [3] developed an adaptive kinematic controller to ensure uniformly ultimately bounded (UUB) set-point regulation, provided conditions on the translational velocity and the bounds on uncertain depth parameters are satisfied. In [4], Conticelli et al. proposed a 3D depth estimation procedure that exploits a prediction error provided a positive definite condition on the interaction matrix is satisfied. In [7] and [8], Fang et al. recently developed 2.5D visual servo controllers to asymptotically regulate a manipulator end-effector and a mobile robot, respectively, by developing an adaptive update law that actively compensates for an unknown depth parameter.

As in [1, 2, 7, 8, 12, 13, 14], the results of this paper are based on exploiting a homography relationship between feature points extracted from images taken by a camera at the reference and current position/orientation. By decomposing the homography into translation and rotation components, geometric relationships are determined that facilitate the construction of an adaptive parameter identification strategy. The development of the parameter identification strategy provides a mechanism to develop visual servo controllers for a newly formulated tracking control problem (all of the aforementioned research has targeted regulating the camera to a fixed position/orientation). Specifically, the tracking control problem is defined as follows: *given some reference posi-*

*This research was supported in part by the U.S. Department of Energy (DOE) Office of Biological and Environmental Research (OBER) Environmental Management Sciences Program (EMSP) project ID No. 82797 at Oak Ridge National Laboratory (ORNL), managed by UT-Battelle, LLC, for the DOE under contract DE-AC05-00OR22725, and in part by a University of Florida subcontract to ORNL by the Florida Department of Citrus, and by U.S. NSF Grant DMI-9457967, ONR Grant N00014-99-1-0589, a DOC Grant, and an ARO Automotive Center Grant.

*tion/orientation of the camera (defined by a reference image), the objective is to track a desired time-varying position/orientation trajectory that is defined in terms of the reference image.* Based on this formulation of the tracking problem, exponential tracking controllers are developed based on the results of the parameter identification strategy. The first tracking controller is developed based on a position-based visual servo (PBVS) control strategy (i.e., the controller only depends on reconstructed task-space information). Motivated by the reported disadvantages of PBVS controllers (see [10, 15] for an in-depth discussion), a 2.5D visual servoing strategy (i.e., the hybrid controller depends on a combination of image-space and reconstructed task-space information) is also developed that yields exponential tracking control.

## 2 Projective Geometry

In this section, geometric relationships are developed between a moving coordinate system (denoted by $\mathcal{F}$) attached to a camera held by the end-effector of a robot manipulator, a desired moving coordinate system (denoted by $\mathcal{F}_d$), a fixed coordinate system (denoted by $\mathcal{F}^*$) that represents a reference position/orientation, and a reference plane $\pi$ that is defined by four target points $O_i$ $\forall i = 1, 2, 3, 4$. Each target point will have a projected pixel coordinate expressed in terms of $\mathcal{F}$ (denoted by $u_i(t)$, $v_i(t) \in \mathbb{R}$), $\mathcal{F}_d$ (denoted by $u_{di}(t)$, $v_{di}(t) \in \mathbb{R}$), and $\mathcal{F}^*$ (denoted by $u_i^*$, $v_i^* \in \mathbb{R}$) that are defined as elements of $p_i(t)$ (actual time-varying image points), $p_{di}(t)$ (desired image point trajectory), and $p_i^*$ (constant reference image points), respectively, as follows

$$p_i \triangleq \begin{bmatrix} u_i & v_i & 1 \end{bmatrix}^T \quad p_{di} \triangleq \begin{bmatrix} u_{di} & v_{di} & 1 \end{bmatrix}^T \quad p_i^* \triangleq \begin{bmatrix} u_i^* & v_i^* & 1 \end{bmatrix}^T. \tag{1}$$

The projected 2D pixel coordinates of the target points introduced in (1) can be related to the 3D task-space coordinates of $O_i$, denoted by $\bar{m}_i(t) \triangleq \begin{bmatrix} X_i(t) & Y_i(t) & Z_i(t) \end{bmatrix}^T \in \mathbb{R}^3$ in $\mathcal{F}$, $\bar{m}_{di}(t) \triangleq \begin{bmatrix} X_{di}(t) & Y_{di}(t) & Z_{di}(t) \end{bmatrix}^T \in \mathbb{R}^3$ in $\mathcal{F}_d$, and $\bar{m}_i^* \triangleq \begin{bmatrix} X_i^* & Y_i^* & Z_i^* \end{bmatrix}^T \in \mathbb{R}^3$ in $\mathcal{F}^*$, by the following transformations

$$p_i = Am_i \qquad p_{di} = Am_{di} \qquad p_i^* = Am_i^* \tag{2}$$

where $A \in \mathbb{R}^{3\times3}$ is a known, constant, and invertible intrinsic camera calibration matrix and $m_i(t)$, $m_{di}(t)$, $m_i^* \in \mathbb{R}^3$, denote the following normalized 3D task-space coordinates of $O_i$ expressed in terms of $\mathcal{F}$, $\mathcal{F}_d$, and $\mathcal{F}^*$, respectively

$$m_i \triangleq \frac{\bar{m}_i}{Z_i} \qquad m_{di} \triangleq \frac{\bar{m}_{di}}{Z_{di}} \qquad m_i^* \triangleq \frac{\bar{m}_i^*}{Z_i^*} \tag{3}$$

where the standard assumption is made that $Z_i(t)$, $Z_{di}(t)$, and $Z_i^*$ are positive. The desired 3D task-space coordinates $\bar{m}_{di}(t)$ are assumed to be first order differentiable.

A projective homography, denoted by $G(t) \in \mathbb{R}^{3\times3}$, can be utilized to relate the image points $p_i(t)$ and $p_i^*$ of (1) in the following manner [9]

$$p_i^* = \alpha_i G p_i \tag{4}$$

where $\alpha_i(t) \in \mathbb{R}$ is an unknown scaling ratio defined as follows

$$\alpha_i \triangleq \frac{Z_i}{Z_i^*} \tag{5}$$

where $Z_i(t)$ and $Z_i^*$ were introduced in (3). From (2) and (4), the following relationship can be developed

$$m_i^* = \alpha_i H m_i \tag{6}$$

where $H(t) \in \mathbb{R}^{3\times3}$ denotes the Euclidean homography that is defined as follows

$$H \triangleq A^{-1}GA\,. \tag{7}$$

The Euclidean homography can be computed using (7) where $G(t)$ is determined by utilizing (4) to solve a linear system of equations using 4 pairs of points $(p_i^*, p_i(t))$ on the reference plane $\pi$ (see [7] for further details). By utilizing various techniques (e.g., see [9, 17]), $H(t)$ can be decomposed as follows

$$H = R + x_h n^T \tag{8}$$

where $R(t) \in SO(3)$ denotes a rotation matrix from $\mathcal{F}$ to $\mathcal{F}^*$, $n(t) \in \mathbb{R}^3$ denotes the unit normal from $\mathcal{F}$ to $\pi$, and $x_h(t) \in \mathbb{R}^3$ denotes a scaled translation vector from $\mathcal{F}^*$ to $\mathcal{F}$ that is expressed in $\mathcal{F}^*$. That is, $R(t)$, $n(t)$, and $x_h(t)$ can be computed from $H(t)$. The translation from $\mathcal{F}^*$ to $\mathcal{F}$, denoted by $x_f(t) \in \mathbb{R}^3$ (expressed in $\mathcal{F}^*$) is unmeasurable; however, it can be expressed in terms of the computed translation vector $x_h(t)$ as follows

$$x_f = x_h d \tag{9}$$

where $d(t) \in \mathbb{R}$ denotes the positive unknown distance from $\mathcal{F}$ to $\pi$ along $n$ (see Figure 1). The translation from $\mathcal{F}^*$ to $\mathcal{F}_d$ is denoted by $x_{fd}(t) \in \mathbb{R}^3$ (expressed in $\mathcal{F}^*$) and is assumed to be first order differentiable (see Figure 1). In Figure 1, $d^*(t) \in \mathbb{R}$ denotes the unknown, constant distance from $\mathcal{F}^*$ to $\pi$ along $n^*(t) \in \mathbb{R}^3$ where $n^*(t)$ denotes the unit normal from $\mathcal{F}^*$ to $\pi$ with coordinates expressed in $\mathcal{F}^*$.

From the expression given in (9), $x_f(t)$ is unmeasurable due to the dependence on the unmeasurable time-varying depth parameter $d(t)$. As a means to compensate for the lack of depth measurements, (9) can be rewritten as follows

$$x_f = \bar{x}_h d^* \tag{10}$$

where the scaled translation signal $\bar{x}_h(t) \in \mathbb{R}^3$ is defined as

$$\bar{x}_h \triangleq \frac{x_h}{\gamma_1}\,. \tag{11}$$

In (11), the positive[1] scaling signal $\gamma_1(t) \in \mathbb{R}$ is defined as follows

$$\gamma_1 \triangleq \frac{d^*}{d} \ . \tag{12}$$

Geometric relationships between $\mathcal{F}$, $\mathcal{F}^*$, and $\pi$ depicted in Figure 1 can be used to develop the following relationship

$$d^* = d + n^{*T} x_f \ . \tag{13}$$

By dividing (13) by $d(t)$, the following measurable expression for $\gamma_1(t)$ can be obtained

$$\gamma_1 = 1 + n^T R^T x_h \tag{14}$$

where the fact that $n^* = R(t)n(t)$ has been used and $n(t)$, $R(t)$, and $x_h(t)$ are computed from (8).

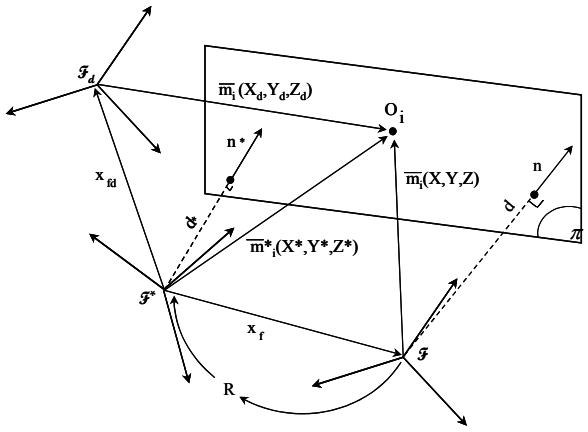


Figure 1: Coordinate frame relationships.

**Remark 1** *A similar homography relationship as in (6) can be developed as follows*

$$m_i^* = \alpha_{di} H_d m_{di} \tag{15}$$

*where* $\alpha_{di} \triangleq Z_{di}/Z_i^*$ *and* $H_d(t) \in \mathbb{R}^{3\times 3}$ *denotes the desired Euclidean homography that can be decomposed as follows*

$$H_d = R_d + x_{hd} n_d^T \tag{16}$$

*where* $R_d(t) \in SO(3)$ *denotes a rotation matrix from* $\mathcal{F}_d$ *to* $\mathcal{F}^*$, $n_d(t) \in \mathbb{R}^3$ *denotes the unit normal from* $\mathcal{F}_d$ *to* $\pi$, *and* $x_{hd}(t) \in \mathbb{R}^3$ *denotes a scaled translation vector from* $\mathcal{F}^*$ *to* $\mathcal{F}_d$ *that is expressed in* $\mathcal{F}^*$.

# 3 Control Objective

The objective is to develop a visual servo controller that ensures $\mathcal{F}$ tracks $\mathcal{F}_d$, where $\mathcal{F}_d$ is moving according to a desired time-varying trajectory that is constructed relative to the reference camera position/orientation given by $\mathcal{F}^*$. To quantify this objective, a rotation tracking error, denoted by $\tilde{e}_\omega(t) \in \mathbb{R}^3$, is defined as follows

$$\tilde{e}_\omega \triangleq e_\omega - e_{\omega d} \ . \tag{17}$$

In (17), $e_\omega(t) \in \mathbb{R}^3$ denotes the rotation mismatch between $\mathcal{F}$ and $\mathcal{F}^*$ with respect to $\mathcal{F}$ and $e_{\omega d}(t) \in \mathbb{R}^3$ denotes the rotation mismatch between $\mathcal{F}_d$ and $\mathcal{F}^*$ with respect to $\mathcal{F}_d$, as follows

$$e_\omega \triangleq u\theta \qquad e_{\omega d} \triangleq u_d \theta_d \tag{18}$$

where $u(t)$, $u_d(t) \in \mathbb{R}^3$ represent unit rotation axes, and $\theta(t), \theta_d(t) \in \mathbb{R}$ denote the respective rotations about $u(t)$ and $u_d(t)$ that are assumed to be confined to the following regions

$$-\pi < \theta(t) < \pi \qquad -\pi < \theta_d(t) < \pi \ . \tag{19}$$

The desired rotation mismatch $e_{\omega d}(t)$ is assumed to be first order differentiable. The parameterization $u(t)\,\theta(t)$ is related to the rotation matrix $R(t)$ (computed from the homography as described in (8)) by the following expression

$$R = I_3 + \sin\theta\,[u]_\times + 2\sin^2\frac{\theta}{2}[u]_\times^2 \tag{20}$$

where the notation $I_i$ denotes an $i \times i$ identity matrix, and the notation $[\zeta]_\times$ denotes the following skew-symmetric cross-product matrix. For details regarding the computation of $u(t)$ and $\theta(t)$ (or $u_d(t)$ and $\theta_d(t)$) from a given rotation matrix $R(t)$ (or $R_d(t)$), see [7].

From a geometric perspective, the position tracking control objective is to force $x_f(t)$ of (9) (see Figure 1) to track the desired time-varying trajectory $x_{fd}(t)$ depicted in Figure 1. To quantify this objective, a position tracking error, denoted by $\tilde{x}_f(t) \in \mathbb{R}^3$, is defined as follows

$$\tilde{x}_f = x_f - x_{fd}. \tag{21}$$

Based on the expressions given in (10), (11), and (14), a measureable relationship for $x_f(t)$ (and hence, $\tilde{x}_f(t)$) can be obtained if the unknown constant parameter $d^*$ can be computed. Motivated by the desire to determine $d^*$, an adaptive calibration routine is developed in the subsequent section and the results of the calibration routine are used to develop several visual servo tracking controllers. To quantify the identification of $d^*$, the parameter estimate error signal $\tilde{d}^*(t) \in \mathbb{R}$ is defined as follows

$$\tilde{d}^* \triangleq d^* - \hat{d}^* \tag{22}$$

where $\hat{d}^*(t) \in \mathbb{R}$ denotes a subsequently designed estimate for $d^*$. To facilitate the development of the adaptive parameter estimation routine, an auxiliary position tracking error, denoted by $\tilde{x}_h(t) \in \mathbb{R}^3$, is defined as the difference between the measurable translation $\bar{x}_h(t)$ defined in (11) and a desired translation $\bar{x}_{hd}(t) \in \mathbb{R}^3$ as follows

$$\tilde{x}_h \triangleq \bar{x}_h - \bar{x}_{hd} \ . \tag{23}$$

[1] The degenerate case when $d(t) = 0$ is assumed to always be avoided.

# 4 Adaptive Parameter Identification

## 4.1 Open-Loop Error System

From Figure 1, the following relationship can be determined

$$\dot{x}_f = R v_c \tag{24}$$

where $v_c(t) \in \mathbb{R}^3$ denotes the linear velocity of the camera expressed in $\mathcal{F}$ and $R(t)$ was introduced in (8). To develop the open-loop error system for $\tilde{x}_h(t)$, we take the time derivative of (23) and multiply the resulting expression by $d^*$ to obtain the following expression

$$d^* \dot{\tilde{x}}_h = R v_c - d^* \dot{\bar{x}}_{hd} \tag{25}$$

where (24) and the time derivative of (10) have been utilized. By selecting the desired trajectory $\bar{x}_{hd}(t)$ as follows (for the identification scheme only)

$$\bar{x}_{hd} \triangleq \begin{bmatrix} \cos(t) & 0 & 0 \end{bmatrix}^T$$

the open loop error dynamics given in (25) can be rewritten as

$$d^* \dot{\tilde{x}}_h = R v_c - d^* \begin{bmatrix} -\sin(t) & 0 & 0 \end{bmatrix}^T . \tag{26}$$

The open-loop error dynamics for $e_\omega(t)$ can be expressed as follows [11, 14]

$$\dot{e}_\omega = -L_\omega \omega_c \tag{27}$$

where $\omega_c(t) \in \mathbb{R}^3$ denotes the angular velocity of the camera expressed in $\mathcal{F}$, and $L_\omega(t) \in \mathbb{R}^{3\times 3}$ is a measurable matrix defined as follows

$$L_\omega \triangleq I_3 + \frac{\theta}{2}[u]_\times + \left(1 - \frac{sinc(\theta)}{sinc^2\left(\frac{\theta}{2}\right)}\right)[u]_\times^2 \tag{28}$$

where

$$sinc(\theta(t)) \triangleq \frac{\sin\theta(t)}{\theta(t)} .$$

**Remark 2** *By exploiting the fact that $u(t)$ is a unit vector (i.e., $\|u\|^2 = 1$), the determinant of $L_\omega(t)$ can be derived as follows [12]*

$$\det L_\omega = \frac{1}{sinc^2\left(\frac{\theta}{2}\right)}, \tag{29}$$

*and it is thus singular only for multiples of $2\pi$ (i.e., out of the assumed workspace).*

## 4.2 Closed-Loop Error System

Based on the structure of the open-loop error systems and subsequent stability analysis, the angular and linear camera velocity control inputs for the range identification problem are defined as follows

$$\omega_c \triangleq k_\omega e_\omega \tag{30}$$

$$v_c \triangleq R^T\left(-k_v \tilde{x}_h + \hat{d}^* \begin{bmatrix} -\sin(t) & 0 & 0 \end{bmatrix}^T\right) \tag{31}$$

where the measureable signals $e_\omega(t)$ and $\tilde{x}_h(t)$ are defined in (18) and (23), respectively. In (30) and (31), $k_v$, $k_\omega \in \mathbb{R}$ denote positive control gains, and $\hat{d}^*(t) \in \mathbb{R}$ denotes the parameter estimate for $d^*$ that is generated by the following differential equation

$$\dot{\hat{d}}^* = -\Gamma \begin{bmatrix} -\sin(t) & 0 & 0 \end{bmatrix} \tilde{x}_h \tag{32}$$

where $\Gamma \in \mathbb{R}$ denotes a positive constant adaptation gain. After substituting (30) into (27) for $\omega_c(t)$ the following closed-loop orientation error system is obtained

$$\dot{e}_\omega = -k_\omega L_\omega e_\omega . \tag{33}$$

After substituting (31) into (26) for $v_c(t)$ the following closed-loop translation error system is obtained

$$d^* \dot{\tilde{x}}_h = -k_v \tilde{x}_h - \tilde{d}^* \begin{bmatrix} -\sin(t) & 0 & 0 \end{bmatrix}^T . \tag{34}$$

## 4.3 Analysis

**Theorem 1** *The adaptive update law defined in (32) along with the control inputs designed in (30) and (31) ensure that the auxiliary error signals $e_\omega(t)$ and $\tilde{x}_h(t)$ are asymptotically driven to zero and that the constant unknown parameter $d^*$ is identified in the sense that*

$$\lim_{t\to\infty} \|e_\omega(t)\|, \ \|\tilde{x}_h(t)\|, \ \tilde{d}(t) = 0 . \tag{35}$$

**Proof:** To prove Theorem 1, we define the following non-negative function

$$V \triangleq \frac{1}{2} e_\omega^T e_\omega + \frac{d^*}{2} \tilde{x}_h^T \tilde{x}_h + \frac{1}{2\Gamma} \tilde{d}^{*2} . \tag{36}$$

After taking the time derivative of (36) and then substituting for the closed-loop error systems developed in (33) and (34), the following expression is obtained

$$\begin{aligned} \dot{V} &= -k_\omega e_\omega^T L_\omega e_\omega + \tilde{d}^* \begin{bmatrix} -\sin(t) & 0 & 0 \end{bmatrix} \tilde{x}_h \\ &\quad + \tilde{x}_h^T \left(-k_v \tilde{x}_h - \tilde{d}^* \begin{bmatrix} -\sin(t) & 0 & 0 \end{bmatrix}^T\right). \end{aligned} \tag{37}$$

By cancelling common terms and utilizing the fact that

$$e_\omega^T L_\omega e_\omega = e_\omega^T e_\omega, \tag{38}$$

the following expression is obtained

$$\dot{V} = -k_\omega e_\omega^T e_\omega - k_v \tilde{x}_h^T \tilde{x}_h . \tag{39}$$

Based on (36) and (39), it can be determined that $e_\omega(t)$, $\tilde{x}_h(t)$, $\tilde{d}^*(t)$, $\hat{d}^*(t) \in \mathcal{L}_\infty$ and that $e_\omega(t)$, $\tilde{x}_h(t) \in \mathcal{L}_2$. The expression given in (30) can be used to conclude that $\omega_c(t) \in \mathcal{L}_\infty$. From (31) - (34), we can now show that $\dot{\hat{d}}(t)$, $v_c(t)$, $\dot{\tilde{x}}_h(t)$, $\dot{e}_\omega(t) \in \mathcal{L}_\infty$. Since $e_\omega(t)$, $\tilde{x}_h(t) \in \mathcal{L}_2$ and $e_\omega(t)$, $\dot{e}_\omega(t)$, $\tilde{x}_h(t)$, $\dot{\tilde{x}}_h(t) \in \mathcal{L}_\infty$, Barbalat's Lemma [16] can be used to prove that

$$\lim_{t\to\infty} \|e_\omega(t)\|, \|\tilde{x}_h(t)\| = 0 \ . \tag{40}$$

The time derivative of (34) can be determined as follows

$$\begin{aligned} d^*\ddot{\tilde{x}}_h &= -k_v\dot{\tilde{x}}_h - \tilde{d}^* \begin{bmatrix} -\cos(t) & 0 & 0 \end{bmatrix}^T \\ &\quad -\dot{\tilde{d}}^* \begin{bmatrix} -\sin(t) & 0 & 0 \end{bmatrix}^T \ . \end{aligned} \tag{41}$$

From (41) and the previous development, $\ddot{\tilde{x}}_h(t) \in \mathcal{L}_\infty$; hence, $\dot{\tilde{x}}_h(t)$ is uniformly continuous (UC). Since $\dot{\tilde{x}}_h(t)$ is UC, (40) and the integral form of Barbalat's Lemma [16] can be used to prove that

$$\lim_{t\to\infty} \left\| \dot{\tilde{x}}_h(t) \right\| = 0 \ . \tag{42}$$

From (34) and the fact that

$$\lim_{t\to\infty} \|\tilde{x}_h(t)\|, \ \left\| \dot{\tilde{x}}_h(t) \right\| = 0,$$

it is clear that

$$\lim_{t\to\infty} \sin(t)\tilde{d}^*(t) = 0 \ . \tag{43}$$

The result given in (43) can be used to prove that the parameter estimate $\hat{d}^*(t)$ can be used to identify the unknown constant parameter $d^*$ in the sense that

$$\lim_{t\to\infty} \tilde{d}^* = 0 \ . \quad \square$$

# 5 Visual Servo Control

Any point $O_i$ on $\pi$ can be utilized in the subsequent development; however, to reduce the notational complexity, we have elected to select the image point $O_1$, and hence, the subscript 1 is utilized in lieu of $i$. Based on the results from Theorem 1, the constant parameter $d^*$ can be actively identified by using the adaptive update law in (32) along with the control inputs designed in (30) and (31). Once $d^*$ has been identified using this procedure, the relationships given in (8), (10), (11), and (14) can be used to compute $x_f(t)$. Moreover, by identifying $d^*$ the unknown time-varying Euclidean depth information $Z_1(t)$ introduced in (2) can be determined. To this end, the auxiliary signal $\gamma_2(t) \in \mathbb{R}$ is defined as follows

$$\gamma_2 \triangleq \frac{Z_1}{d^*} \ . \tag{44}$$

Based on the fact that $d(t)$ is equal to the projection of $\bar{m}_1(t)$ along $n(t)$ as follows (see Figure 1)

$$d = n^T\bar{m}_1, \tag{45}$$

(3) and (12) can be used to rewrite (44) in the following measurable form

$$\gamma_2 = \frac{1}{n^T m_1 \gamma_1} \quad \text{hence,} \quad Z_1 = \frac{d^*}{n^T m_1 \gamma_1} \tag{46}$$

where the measureable form of $\gamma_1(t)$ is given in (14). These facts will be utilized in the development of the subsequent controllers.

## 5.1 PBVS Tracking Controller

After taking the time derivative of (21) the following expression is obtained

$$\dot{\tilde{x}}_f = Rv_c - \dot{x}_{fd} \tag{47}$$

where (24) was utilized, and $\dot{x}_{fd}(t)$ denotes the time derivative of $x_{fd}(t)$ introduced in (21). The open-loop tracking error dynamics for $\tilde{e}_\omega(t)$ are determined by taking the time derivative of (17) as follows

$$\dot{\tilde{e}}_\omega = -L_\omega\omega_c - \dot{e}_{\omega d} \tag{48}$$

where (27) was utilized, and $\dot{e}_{\omega d}(t)$ denotes the time derivative of the desired mismatch introduced in (17). From (47) and (48), the linear and angular velocity control inputs for the camera are designed as follows

$$v_c \triangleq R^T\left(\dot{x}_{fd} - k_v\tilde{x}_f\right) \qquad \omega_c \triangleq L_\omega^{-1}\left(-\dot{e}_{\omega d} + k_\omega\tilde{e}_\omega\right) \ . \tag{49}$$

After substituting (49) into (47) and (48) and then solving the resulting differential equations, the transient and steady state response of the position/orientation tracking errors can be proven to be confined to the following exponentially decaying envelopes

$$\tilde{x}_f(t) = \tilde{x}_f(0)\exp(-k_v t) \qquad \tilde{e}_\omega(t) = \tilde{e}_\omega(0)\exp(-k_\omega t) \ . \tag{50}$$

Standard signal chasing arguments can now be used to prove that signals are bounded under closed-loop operation.

## 5.2 2.5D Tracking Control

To develop a 2.5D visual servo controller, a new hybrid position tracking error, denoted by $e_v(t) \in \mathbb{R}^3$, is defined as follows

$$e_v \triangleq m_e - m_{ed} \tag{51}$$

where $m_e(t) = \begin{bmatrix} m_{e1}(t) & m_{e2}(t) & m_{e3}(t) \end{bmatrix}^T \in \mathbb{R}^3$ denotes the coordinates of an image point on $\pi$ extended by the Euclidean depth coordinate as follows

$$m_e \triangleq \begin{bmatrix} \dfrac{X_1}{Z_1} & \dfrac{Y_1}{Z_1} & Z_1 \end{bmatrix}^T \tag{52}$$

and $m_{ed}(t) = \begin{bmatrix} m_{ed1}(t) & m_{ed2}(t) & m_{ed3}(t) \end{bmatrix}^T \in \mathbb{R}^3$ denotes the extended image coordinates of the corresponding desired image point as follows

$$m_{ed} \triangleq \begin{bmatrix} \dfrac{X_{d1}}{Z_{d1}} & \dfrac{Y_{d1}}{Z_{d1}} & Z_{d1} \end{bmatrix}^T \tag{53}$$

where $X_{d1}(t)$, $Y_{d1}(t)$, and $Z_{d1}(t)$ denote the time-varying coordinates introduced in (2).

After taking the time derivative of (51), the following expression can be obtained

$$\dot{e}_v = \dot{m}_e - \dot{m}_{ed} = \frac{1}{Z_1} \begin{bmatrix} 1 & 0 & -m_{e1} \\ 0 & 1 & -m_{e2} \\ 0 & 0 & m_{e3} \end{bmatrix} \dot{\bar{m}}_1 - \dot{m}_{ed} \quad (54)$$

where $\dot{\bar{m}}_1(t)$ is given by the following expression [7]

$$\dot{\bar{m}}_1 = -v_c + \bar{m}_1^{\times} \omega_c \ . \quad (55)$$

After substituting (55) into (54), the following open-loop tracking error system can be developed

$$\dot{e}_v = \frac{1}{Z_1} L_v v_c + L_{v\omega} \omega_c - \dot{m}_{ed} \quad (56)$$

where $L_v(t)$, $L_{v\omega}(t) \in \mathbb{R}^{3\times 3}$ are defined as follows

$$L_v \triangleq \begin{bmatrix} -1 & 0 & m_{e1} \\ 0 & -1 & m_{e2} \\ 0 & 0 & -m_{e3} \end{bmatrix}$$

$$L_{v\omega} \triangleq \begin{bmatrix} m_{e1}m_{e2} & -1-m_{e1}^2 & m_{e2} \\ 1+m_{e2}^2 & -m_{e1}m_{e2} & -m_{e1} \\ -m_{e2}m_{e3} & m_{e1}m_{e3} & 0 \end{bmatrix} .$$

Based on the open-loop error system in (56), the camera linear velocity input is designed as follows

$$v_c \triangleq Z_1 L_v^{-1} \left(-k_v e_v - L_{v\omega}\omega_c + \dot{m}_{ed}\right) \quad (57)$$

where $Z_1(t)$ can be computed from the expression given in (46). After substituting (57) into (56) and then solving the resulting differential equation, the transient and steady state response of the position tracking error introduced in (51) can be proven to be confined to the following exponentially decaying envelope

$$e_v(t) = e_v(0)\exp(-k_v t) \ . \quad (58)$$

By designing $\omega_c(t)$ as in (49), the rotation tracking error can be proven to be confined to the same exponentially decaying envelope as in (50). Standard signal chasing arguments can now be used to prove that signals are bounded under closed-loop operation.

# 6 Conclusion

A projective homography is developed by exploiting the geometric relationships between coordinate frames attached to the current and a reference camera position/orientation. The relationships are exploited to facilitate the construction of an adaptive strategy to identify unknown depth information. Once the constant unknown depth parameter is identified, geometric relationships are exploited to determine several time-varying depth related signals. By determining these signals, PBVS and 2.5D visual servo tracking controllers are designed. Both visual servoing controllers are proven to yield exponential tracking.

# References


[1] F. Chaumette and E. Malis, "2 1/2 D Visual Servoing: A Possible Solution to Improve Image-based and Position-Based Visual Servoings," *Proc. of the IEEE International Conference on Robotics and Automation*, May 2000, pp. 630-635.

[2] F. Chaumette, E. Malis, and S. Boudet, "2D 1/2 Visual Servoing with Respect to a Planar Object," *Workshop on New Trends in Image-Based Robot Servoing*, 1997, pp. 45-52.

[3] F. Conticelli and B. Allotta, "Nonlinear Controllability and Stability Analysis of Adaptive Image-Based Systems," *IEEE Trans. on Robotics and Automation*, 17(2), 2001, pp. 208-214.

[4] F. Conticelli and B. Allota, "Discrete-Time Robot Visual Feedback in 3-D Positioning Tasks with Depth Adaptation," *IEEE Trans. on Mechatronics*, 6(3), 2001, pp. 356-363.

[5] P. I. Corke and S. A. Hutchinson, "A New Hybrid Image-Based Visual Servo Control Scheme," *Proc. of the IEEE Conference on Decision and Control*, Dec. 2000, pp. 2521-2527.

[6] K. Deguchi, "Optimal Motion Control for Image-Based Visual Servoing by Decoupling Translation and Rotation," *Intl. Conf. on Intelligent Robots and Systems*, 1998, pp. 705-711.

[7] Y. Fang, A. Behal, W. E. Dixon and D. M. Dawson, "Adaptive 2.5D Visual Servoing of Kinematically Redundant Robot Manipulators," *Proc. of the IEEE Conference on Decision and Control,* Dec. 2002, pp. 2860-2865.

[8] Y. Fang, D. M. Dawson, W. E. Dixon, and M. S. de Queiroz, "2.5D Visual Servoing of Wheeled Mobile Robots," *Proc. of the IEEE Conf. on Decision and Control*, 2002, pp. 2866-2871.

[9] O. Faugeras and F. Lustman, "Motion and Structure from Motion in a Piecewise Planar Environment," *International Journal of Pattern Recognition and Artificial Intelligence,* 2(3), 1988 , pp. 485-508.

[10] G. D. Hager and S. Hutchinson (guest editors), Special Section on Vision-Based Control of Robot Manipulators, *IEEE Trans. Robotics and Automation*, 12(5), Oct. 1996.

[11] E. Malis, "Contributions à la Modélisation et à la Commande en Asservissement Visuel," *Ph.D. Dissertation*, University of Rennes I, IRISA, France, Nov. 1998.

[12] E. Malis and F. Chaumette, "Theoretical Improvements in the Stability Analysis of a New Class of Model-Free Visual Servoing Methods," *IEEE Transactions on Robotics and Automation*, 18(2), April 2002, pp. 176-186.

[13] E. Malis and F. Chaumette, "2 1/2 D Visual Servoing with Respect to Unknown Objects Through a New Estimation Scheme of Camera Displacement," *International Journal of Computer Vision*, 37(1), June 2000, pp. 79-97.

[14] E. Malis, F. Chaumette, and S. Bodet, "2 1/2 D Visual Servoing," *IEEE Transactions on Robotics and Automation*, 15(2), April 1999, pp. 238-250.

[15] B. Nelson and N. Papanikolopoulos (guest editors), Special Issue of Visual Servoing, *IEEE Robotics and Automation Mag.*, 5(4), Dec. 1998.

[16] J. J. E. Slotine and W. Li, *Applied Nonlinear Control*, Prentice Hall, Inc, Englewood Cliff, NJ, 1991.

[17] Z. Zhang and A. R. Hanson, "Scaled Euclidean 3D Reconstruction Based on Externally Uncalibrated Cameras," *IEEE Symp. on Computer Vision*, 1995, pp. 37-42.